



Scaling of potential evapotranspiration with MODIS data reproduces flux observations and catchment water balance observations across Australia

Juan Pablo Guerschman^{a,*}, Albert I.J.M. Van Dijk^a, Guillaume Mattersdorf^a, Jason Beringer^b, Lindsay B. Hutley^c, Ray Leuning^d, Robert C. Pipunic^e, Brad S. Sherman^a

^a CSIRO Land and Water, GPO Box 1666, Canberra, ACT 2601, Australia

^b School of Geography and Environmental Science, Monash University, P.O. Box 11A, Clayton, VIC 3800, Australia

^c School of Environmental and Life Sciences, Charles Darwin University, Darwin, NT 0909, Australia

^d CSIRO Marine and Atmospheric Research, GPO Box 3023, Canberra, ACT 2601, Australia

^e Department of Civil and Environmental Engineering, The University of Melbourne, Parkville VIC 3010, Australia

ARTICLE INFO

Article history:

Received 30 May 2008

Received in revised form 2 February 2009

Accepted 9 February 2009

This manuscript was handled by K. Georgakakos, Editor-in-Chief, with the assistance of V. Lakshmi, Associate Editor

Keywords:

Evapotranspiration

Remote sensing

MODIS

Australia

SUMMARY

We developed a new algorithm for estimating monthly actual evapotranspiration (AET) based on surface reflectance from MODIS-Terra and interpolated climate data. The algorithm uses monthly values of the Enhanced Vegetation Index (EVI) and the Global Vegetation Moisture Index (GVMI) derived from the MODIS nadir bidirectional reflectance distribution function – adjusted reflectance product (MOD43B4) to scale Priestley–Taylor potential evapotranspiration derived from the climate surfaces. The EVI is associated with evapotranspiration through its relationship with leaf area index. The GVMI allows separation between surface water and bare soil when EVI is low and provides information on vegetation water content when EVI is high. The model was calibrated using observed AET data from seven sites in Australia, including two forests, two open savannas, a grassland, a floodplain and a lake. Model outputs were compared with four year average difference between precipitation and streamflow (a surrogate for mean AET) in 227 unimpaired catchments across Australia. We tested four different model configurations and found that the best results both in the calibration and evaluation datasets were obtained when a precipitation interception term (E_i) and the GVMI were incorporated into the model. The E_i term and the GVMI improved AET estimates in the forest, savanna and grassland sites and in the lake and floodplain sites respectively. The most comprehensive model estimated monthly AET at the seven calibration sites with a RMSE of 18.0 mm mo⁻¹ (22% of the mean AET, $r^2 = 0.84$). In the evaluation dataset, mean annual AET was estimated with a RMSE of 137.44 mm y⁻¹ (19% of the mean AET, $r^2 = 0.61$). The model was able to reproduce the main spatial and temporal patterns in AET across Australia. The main advantages of the proposed model are that it uses a single set of parameters (i.e. does not need an auxiliary land cover map) and that it is able to estimate AET in areas with significant direct evaporation, including lakes and floodplains.

Crown Copyright © 2009 Published by Elsevier B.V. All rights reserved.

Introduction

Australia's vital water resources are characterised by a high level of use and a large seasonal and annual variability in precipitation, soil moisture and the consequent recharge of surface and groundwater. The precarious state of water resources availability has been highlighted in recent years, as large parts of eastern Australia suffered one of the worst droughts in recorded history (Alexander et al., 2007; Liu et al., 2007). More sustainable and efficient use of water resources requires accurate knowledge of the generation and distribution of these resources.

Generation of soil, surface and groundwater resources is the difference between precipitation (P) and evapotranspiration (ET). In many parts of Australia this is a small difference between two large terms, and therefore accurate estimates of P and ET are essential to improve precision of surface and groundwater hydrological models. Total ET includes plant transpiration and direct evaporation from wet canopy and litter, the soil and water surfaces. Local measurements of transpiration can be made using sap flow techniques, whereas total ET can be measured using micrometeorological techniques such as the eddy covariance method, or lysimeters, site or catchment water balance techniques (for comparisons see Ford et al., 2007; Kosugi and Katsuyama, 2007; Wilson et al., 2001). These methods allow excellent temporal (hourly) resolution but are limited spatially. At landscape scales, the only feasible approach to estimating ET with a reasonable degree of accuracy is

* Corresponding author. Tel.: +61 2 6246 5880; fax: +61 2 6246 5988.

E-mail address: Juan.Guerschman@csiro.au (J.P. Guerschman).

through the use of remote sensing techniques. Remote sensing methods typically rely on the relation between ET and surface temperature or on the relationship between vegetation cover and ET (see e.g. Glenn et al., 2007 and Mu et al., 2007, for an overview of approaches). Vegetation indices such as NDVI, EVI and leaf area index (LAI) estimates derived from either of these indices have proven promising when used in a surface energy and water balance model such as the Penman–Monteith equation (e.g. Cleugh et al., 2007; Leuning et al., 2008; Mu et al., 2007; Zhang et al., 2008).

However there is room for improvement. In general the existing methods that rely on vegetation indices only estimate the transpiration component (T) and not the contribution of direct evaporation (E) to ET (Glenn et al., 2007). In the extreme case of open water surfaces these methods would estimate zero ET. More recently an explicit accounting of direct evaporation from bare soils was introduced in a semi-empirical model which can also cope with evaporation from water (Leuning et al., 2008). Another constraint imposed in models that attempt to estimate ET at regional to global scales is the need of a land cover map because such models are generally parameterised separately for different vegetation classes.

Existing algorithms typically do not attempt to estimate precipitation interception losses (E_i) which can contribute significantly to overall ET and can be an important reason for differences in observed water use between short (crops) and tall (forest) vegetation (van Dijk and Keenan, 2007). In extreme cases E_i can even exceed transpiration (e.g. in humid coastal areas; Schellekens, 2000; Shuttleworth and Calder, 1979; Wallace and McJannet, 2008). Interpretation of forest water balance measurements have repeatedly suggested evaporation rates from wet canopies can significantly exceed those expected from meteorological observations (e.g. earlier references and Deguchi et al., 2006; van Dijk and Bruijnzeel, 2001a, 2001b). Radiation energy is typically small during and shortly after storms (whether they occur by day or night) and therefore proposed mechanisms for high rates of ET tend to invoke heat advection (e.g. from a warmer nearby ocean) or problems in measuring air moisture deficit during precipitation, or an effective lowering of aerodynamic resistance due to vertical wind gusts or the mechanical dispersal of precipitation droplets upon hitting the canopy (Murakami, 2006).

Alternative ET estimation methods use a scaling factor or ‘crop coefficient’ specific for a particular vegetation type and condition (e.g. crop stage) in combination with a reference or potential ET. Reference ET can be measured with evaporation pans or similar devices, or estimated from meteorological observations using the Penman or Penman–Monteith model (e.g. with standard parameters representing open water or a well-watered crop or grass cover) or simply as equilibrium evaporation (i.e. net available energy). One such measure was developed in Australia by Priestley and Taylor (1972) who found that ET from well-watered vegetation and open water (measured using lysimeters and micrometeorological methods) was on average about 1.26 times (range 1.08–1.34) greater than equilibrium evaporation and they proposed this as a useful estimate of reference ET that was also in agreement with maximum temperatures observed over wet surfaces (Priestley, 1966). The multiplier effectively accounts for the aerodynamic contribution to total ET of entrainment of dry air at the top of the planetary boundary layer into the surface boundary layer (Raupach, 1995). Although typically not favoured in meteorological applications due to their empirical nature, scaling methods have been shown to be a simple but powerful technique to estimate ET in agronomical and hydrological applications (e.g. Doorenbos and Pruitt, 1977).

In this paper, we seek to develop an ET estimation method that provides accurate estimates of ET from diverse land covers and that accounts for all sources of ET, including transpiration

as well as soil and water evaporation and wet canopy evaporation. We do this implicitly by including indices of vegetation greenness (EVI) and moisture availability in the canopy and at the surface (GVMI) calculated from MODIS reflectance data, and combining these with gridded monthly estimates of Priestley–Taylor reference ET and P . The model is based on the reference ET scaling method and therefore largely empirical. A specific desired characteristic of the model is to be independent of land cover type, i.e., the calibration of the model (parameters) should be the same for all land cover types, including vegetated and non-vegetated surfaces, and not rely on land cover classification.

We explored the effects on the overall model performance of including in the model structure a surface water content index and the water interception term. Following Van Dijk and Mattersdorf, 2007, our hypothesis is that the inclusion of these terms in the model structure will lead to a better estimation of AET. The model was calibrated using monthly evapotranspiration measurements obtained in seven sites across Australia (six vegetated sites of which one is a seasonally flooded wetland and one open water site) and the model performance at the catchment scale was evaluated using streamflow data from 227 unimpaired (unregulated) catchments in Australia. The AET estimates obtained have a spatial resolution of 1 km, cover the whole Australian continent and have a monthly temporal step, beginning in February 2000.

Methods

Field observations of actual evapotranspiration

Field measurements of AET from seven sites in Australia were used for calibrating the model described in “AET model structure”. Table 1 summarises the data used and Fig. 1 shows the site locations. The data obtained from the sites detailed in Table 1 included measurements of latent heat flux (λE) and air temperature. The data were provided by the principal researcher for each flux tower as half-hourly, daily or monthly averages. Where gaps were not already filled, this was done using linear interpolation for small gaps and substitution with the diurnal average of surrounding days for larger gaps (cf. (Falge et al., 2001; Van Dijk and Dolman, 2004)). Where more than 50% of data was missing for a month the average flux for this month was discarded from the analyses. Monthly average λE values were converted to daily ET rates using λ values calculated from mean air temperature.

Falge et al. (2001) analysed the uncertainty introduced by alternative gap-filling strategies and estimated this at approximately 10% of the monthly average for a typical missing data percentage of 30%. Another important source of uncertainty in flux tower data is the energy balance closure problem. Wilson et al. (2002) reviewed flux observations for 22 sites globally and estimated that this results in an uncertainty of about 20% on average in λE , at a 30-min time step, with underestimation of real λE being most likely in the majority of cases. On the whole, an error of about 10–20% in monthly ET rates and an underestimation may perhaps be expected, but systematic differences between sites are likely. For example, Leuning et al. (2005) reported an energy balance closure within 10% for the Tumbarumba and Virginia Parks sites. A similar degree of energy balance closure (~11%) is observed at the Howard Springs site (J. Beringer, L. Hutley, pers. comm.).

MODIS data

The nadir BRDF-adjusted reflectance (NBAR) product (MOD43B4) provides a 16-day, 1 km average reflectance corrected for bidirectional reflectance distribution function (BRDF) and

Table 1

Description of the sites where AET was measured. Data from these sites were used for calibrating the AET model. The measurements were taken with an eddy covariance, open path sensor in all sites, with the exception of Hume Dam where a Stability-corrected bulk formulae. (Liu et al., 1979) was used. Mean annual potential evapotranspiration (PET) and precipitation (P) are reported for the period 2000–2006. P was obtained from the SILO database (Jeffrey et al., 2001) and PET from (Raupach et al., 2001).

Site name (abbreviation)	Location (lat/lon) elevation [m.a.s.l.]	Land cover type	Mean annual PET mean annual precipitation % of months with P > PET	Measurement period (number of months)	Reference
Tumbarumba (Tumb)	–35.65572 148.15208 1200	Wet open sclerophyll forest	1198 mm y ^{–1} 1027 mm y ^{–1} 44%	Feb 2002–Apr 2005 (49)	Leuning et al. (2005)
Virginia Park (ViPa)	–19.88330 146.55389 290	Open woodland savanna	1884 mm y ^{–1} 524 mm y ^{–1} 7%	Jul 2001–Feb 2003 (20)	Leuning et al. (2005)
Howard Springs (HoSp)	–12.49520 131.15005 37	Open forest savanna	2076 mm y ^{–1} 1764 mm y ^{–1} 31%	Aug 2001–Aug 2006 (56)	Beringer et al. (2007) and Beringer et al. (2003)
Wallaby Creek (Wall)	–37.43333 145.18333 685	Mountain ash forest	1122 mm y ^{–1} 1035 mm y ^{–1} 50%	Aug 2005–Dec 2006 (16)	Martin et al. (2007) and Wood et al. (2008)
Kyeamba (Kyem)	–35.32395 147.53480 232	Grassland	1510 mm y ^{–1} 502 mm y ^{–1} 23%	Jan 2005–Dec 2005 (12)	http://www.oznet.unimelb.edu.au/k10.html
Fogg Dam (Fogg)	–12.54250 131.30690 4	Floodplain	2084 mm y ^{–1} 1566 mm y ^{–1} 27%	Nov 2005–Dec 2006 (14)	Hutley and Beringer (unpublished)
Hume Dam (Hume)	–36.10786 147.03329 180	Reservoir lake (open water)	1435 mm y ^{–1} 603 mm y ^{–1} 25%	Nov 2001–May 2003 (12)	Sherman (2005)

atmospheric effects, creating an apparent reflectance that is not affected by the location of the sensor relative to the pixel at the time of acquisition (Schaaf et al., 2002) and is ideally suited for developing a product for monitoring vegetation condition over large areas. We obtained the full series of MOD43B4, collection four data for the Australian continent from 2000 to 2006. The MOD43B4 product is generated using the Terra sensor (overpass ~10.40 AM local time). The image tiles were mosaicked and rectified to a geographical projection using the MODIS reprojection tool. The images were acquired and processed by CSIRO and full details of the process can be found in Paget and King (2008). We reprocessed the 16 day composites into monthly composites using a weighted averaging method:

$$\rho_m = \sum_{i=1}^{2or3} \rho_i \cdot p_{i/m} \quad (1)$$

where ρ_m is the reflectance in the month m , ρ_i is the reflectance in the 16-day composite i and $p_{i/m}$ is the proportion of days of month m included in the 16-day composite i . If one of the two or three ρ_i included in the month was masked because of cloud contamination and the $p_{i/m}$ for that composite was lower than 0.3, the monthly reflectance was calculated ignoring that 16-day composite. If in the previous case $p_{i/m}$ was higher than 0.3 or there were two or three masked ρ_i in that particular month then the resulting ρ_m was masked. This method was applied to the seven reflectance bands included in the MODIS NBAR dataset. The new dataset generated is referred from here on as “monthly NBAR”.

A Residual moisture index (RMI)

A Residual Moisture Index (RMI) was developed by combining the Enhanced Vegetation Index (EVI) (Huete et al., 2002) and the Global Vegetation Moisture Index (GVMI) (Ceccato et al., 2002a, 2002b):

$$EVI = G \cdot \frac{\rho_{NIR} - \rho_{red}}{\rho_{NIR} + C_1 \cdot \rho_{red} - C_2 \cdot \rho_{blue} + L} \quad (2)$$

$$GVMI = \frac{(\rho_{NIR} + 0.1) - (\rho_{SWIR2} + 0.02)}{(\rho_{NIR} + 0.1) + (\rho_{SWIR2} + 0.02)} \quad (3)$$

where ρ_{red} , ρ_{NIR} , ρ_{blue} and ρ_{SWIR2} are the reflectances in red (645 nm), near-infrared (860 nm), blue (469 nm) and shortwave infrared (1640 nm) respectively and correspond to MODIS bands 1, 2, 3 and 6. In the EVI formula, G , C_1 , C_2 and L are parameters that account for aerosol scattering and absorption and their values are 2.5, 6, 7.5 and 1, respectively as described by Huete et al. (2002). The EVI and GVMI were calculated for each composite using the monthly NBAR data described above.

The EVI is an index of vegetation greenness that has been used for estimating vegetation biomass, leaf area index (LAI) and productivity (e.g. Myneni et al., 2007; Nemani et al., 2003). It is calculated using the red-near infrared absorption feature from green vegetation in a similar manner as the Normalised Difference Vegetation Index (NDVI) but it also incorporates some corrections for minimising the saturation effects shown by the NDVI at high LAI values. The GVMI was developed for estimating vegetation water content using the radiative transfer model PROSPECT (Ceccato et al., 2002a) and then tested in several vegetated sites in Senegal (Ceccato et al., 2002b). These authors showed that the GVMI is asymptotically related to the equivalent water thickness at the canopy level.

We explored the distribution of pixels from the field sites in the space defined by the EVI and the GVMI and also the spatial distribution of pixels in the Australian continent. The two indices were able to discriminate vegetated areas from open water surfaces and also split vegetation types into separate clusters (Fig. 2). As both the EVI and the GVMI respond positively to increases in near-infrared reflectance, the two indices had a relatively high correlation. If the correlation between the two indices is removed, the residuals could be used as an indicator of vegetation moisture. We hypothesise that incorporating these residuals into an evaporation model would improve the model performance as the vegetation moisture content can be used as a surrogate for canopy conductance and because open water surfaces can be separated from bare soil and vegetation. A previous analysis by Mattersdorf (unpublished) also explored two other widely used moisture content indices (the Land Surface Wetness Index (LSWI) (Xiao et al., 2002) and the Moisture Stress Index (MSI) (Doraiswamy and Thompson, 1982) but those indices provided a lower ability to discriminate the land cover types of interest here when used with the EVI.

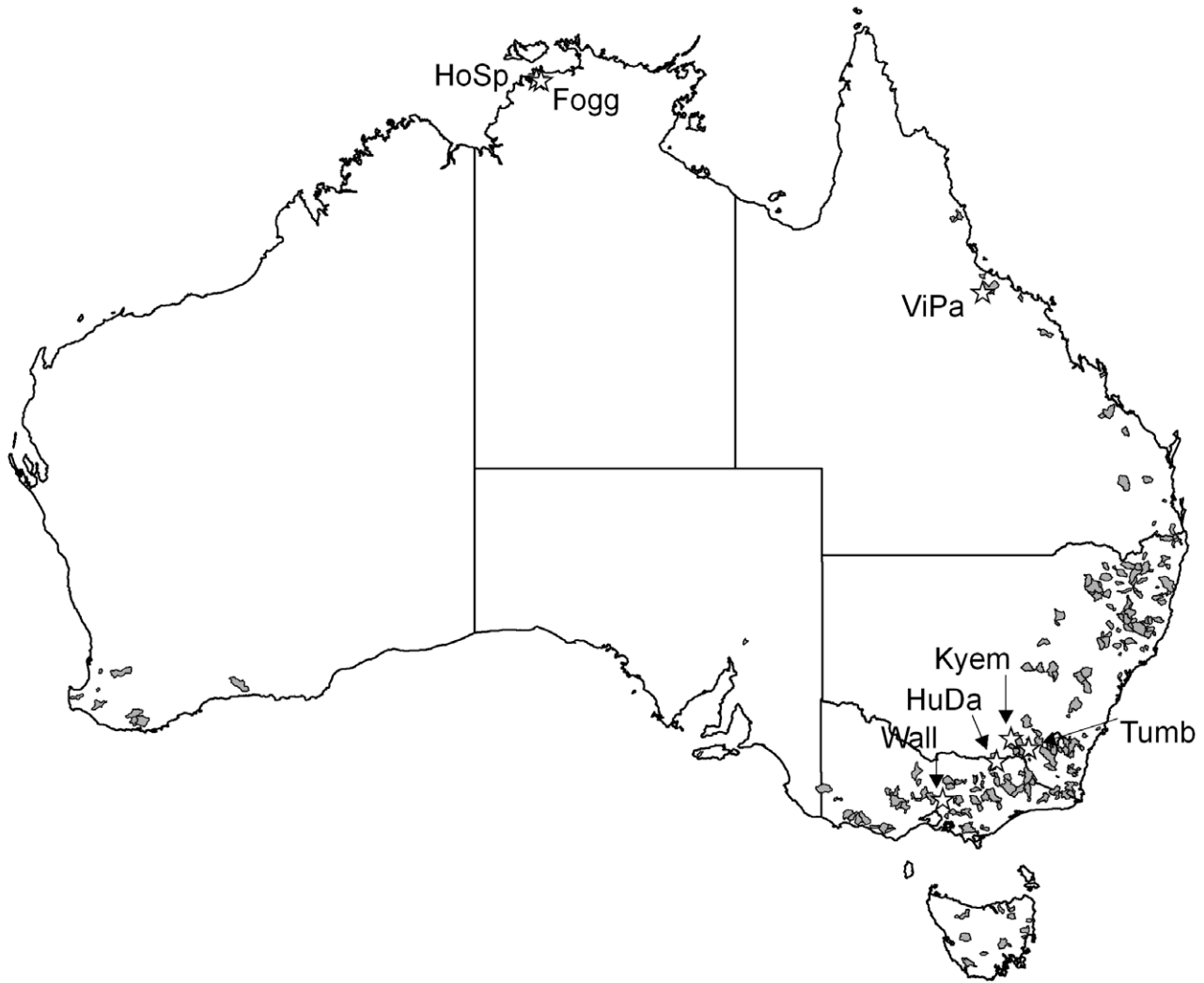


Fig. 1. Map of Australia showing the location of the seven sites with field measurements of AET (stars) used for calibration and the 227 unimpaired catchments (grey polygons) used for model evaluation.

The Residual Moisture Index (RMI) was calculated for each pixel as the vertical distance between its corresponding GVMI and a baseline (Fig. 2). In this way, we eliminated most of the correlation between the two indices and captured the vegetation moisture content and also the particular features observed in open water surfaces. We first determined the intercept and slope of the linear function:

$$GVMI = K_{RMI} \cdot EVI + C_{RMI} \quad (4)$$

and then, for a given pixel we calculated RMI as the vertical distance to the line defined above as:

$$RMI = \max(0, GVMI - (K_{RMI} \cdot EVI + C_{RMI})) \quad (5)$$

The exact position of the baseline is given by the parameters C_{RMI} and K_{RMI} . We estimated these parameters simultaneously with the calibration of the AET model as explained in “Model calibration”.

Using the monthly NBAR images the EVI and the GVMI were calculated and time series of EVI and GVMI for each field site was obtained from their corresponding pixel. We compared the resulting time series of EVI and GVMI obtained by this method with the alternative of using the mean of a 3×3 and 5×5 pixel window centred on the site and obtained very similar results.

AET model structure

With the aim of exploring and comparing the effects of the inclusion of the RMI and a term representing precipitation interception (E_i) in the model structure we designed four different alternative model configurations. We refer hereafter to the four model configurations as 1a, 1b, 2a and 2b where the number indicates whether the RMI is used or not and the letter indicates the inclusion of the E_i term. The first, simplest, model (1a) had the following structure:

$$AET = k_C \cdot PET \quad (6)$$

where k_C is the “crop factor” that represents the ratio of actual to potential evapotranspiration and PET is the potential evapotranspiration, obtained from climatic data (explained in “Climate data”). The crop factor k_C is given by:

$$k_C = k_{MAX} \cdot [1 - \exp(-a \cdot EVI_r^2)] \quad (7)$$

where k_{MAX} is the maximum value for the crop factor and EVI_r is the rescaled EVI.

This model configuration gives a sigmoidal that makes k_C range from zero when EVI_r equals zero to k_{MAX} when EVI_r equals one. The exact shape of the sigmoid is determined by the parameters a and

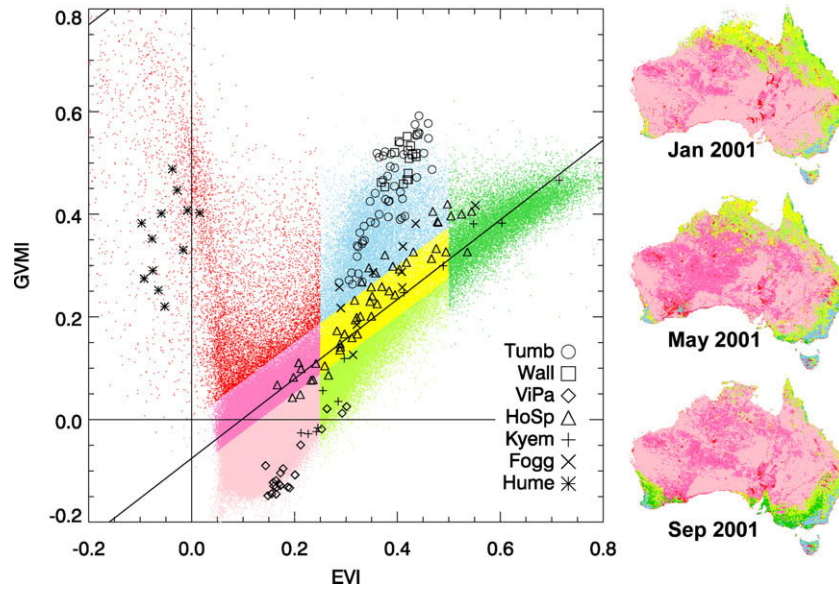


Fig. 2. Scatterplot of the Global Vegetation Moisture Index (GVMI) and the Enhanced Vegetation Index (EVI) in the seven sites with AET observations. Each symbol corresponds to a month in the corresponding site. The colored dots in the background show the distribution of pixels in the Australian continent for the month of September 2001. The classes were arbitrarily defined with the purpose of showing the spatial distribution of EVI and GVMI in different dates. The inset maps show the location of the pixels indicated by the colored classes in the scatterplot for the months of January, May and September 2001. The Residual Moisture Index (RMI) was calculated as the distance in the GVMI axis of a given pixel to a line defined as $GVMI = C_{RMI} + K_{RMI}$. The parameters C_{RMI} and K_{RMI} were fitted during the model calibration. The line shown in the graph corresponds to the baseline fitted in model variant 2b.

α , which were, together with k_{MAX} , adjusted empirically during the calibration process, as explained in “Model calibration”. The re-scaled EVI was calculated as:

$$EVI_r = \frac{EVI - EVI_{min}}{EVI_{max} - EVI_{min}} \quad (8)$$

with $EVI_{min} = 0$ and $EVI_{max} = 0.90$. EVI_r was capped at 0 when $EVI < EVI_{min}$ and capped at 1 when $EVI > EVI_{max}$.

The second model (1b) incorporated a representation of precipitation lost through interception (water evaporated directly from the vegetation surface, E_i) and had the following formulation:

$$AET = k_C \cdot PET + k_{Ei} \cdot P \quad (9)$$

where k_{Ei} is a term that quantifies E_i and P is the monthly precipitation. The term k_C was calculated as in Eq. (9). k_{Ei} was linearly related to EVI_r following:

$$k_{Ei} = k_{Ei_{max}} \cdot EVI_r \quad (10)$$

The models 2a and 2b were equivalent to 1a and 1b respectively, but also included the RMI in the calculation of k_C :

$$k_C = k_{C_{max}} \cdot (1 - \exp(-a \cdot EVI_r^\alpha - b \cdot RMI^\beta)) \quad (11)$$

In the equation above the term $k_{C_{max}}$ is multiplied by a sigmoidal function that depends simultaneously on EVI_r and RMI.

The four model variants described above allowed an analysis of the improvements in the model function by including E_i (comparing the performance of models a and b), by including the RMI (models 1 and 2), and by including both the E_i and RMI (models 1a and 2b).

Climate data

Climate data were obtained from the SILO dataset which contains daily climate variables interpolated from meteorological stations and covers the entire Australian continent at a spatial resolution of 0.05 degrees (~ 5 km at 30° S). A comprehensive description of SILO, including the interpolation techniques and de-

tails about its accuracy can be found in Jeffrey et al. (2001). We used the Priestley-Taylor potential evapotranspiration (PET) grids produced by Raupach et al. (2001) from daily temperature and radiation in the above mentioned SILO dataset following the equation:

$$PET = \frac{\alpha}{\lambda} \frac{\Delta}{\Delta + \gamma} (R_n - G) \quad (12)$$

where R_n is the net radiation ($MJ m^{-2} day^{-1}$), G is the soil heat flux (assumed to be 0), Δ is the slope of the vapour pressure-temperature curve ($kPa K^{-1}$), γ is the psychrometric constant ($\sim 66 Pa K^{-1}$), λ is the latent heat of evaporation ($\sim 2.5 \cdot 10^6 J mm^{-1}$), and α is an empirical factor of 1.26 (Priestley and Taylor, 1972). Like any formulation of PET, Priestley-Taylor PET is a hypothetical measure of evaporative demand. The Priestley-Taylor formulation was chosen because of its clear physical interpretation and the fact that it does not require wind speed, of which accurate estimates were not available at the continental scale at the time of this analysis (although a recent paper by McVicar et al., 2008 produced such database). Some experimental and theoretical studies have suggested that better estimates of α would be up to 1.32 (e.g. Morton, 1983; Hobbins et al., 2001). A uniform proportional bias arising from this would be compensated through model calibration. Daily precipitation from the SILO dataset and PET were aggregated to the monthly scale and then over-sampled to a spatial resolution of 1 km in order to match the temporal and spatial resolution of the MODIS imagery.

Model calibration

For each variant the model was calibrated by searching for the values of the parameters that minimised the objective function:

$$J = \sum_{i,j} (AET_{Oij} - AET_{Mij})^2 \quad (13)$$

where AET_{Oij} and AET_{Mij} are the observed (from field measurements) and modelled (model outputs) AET in the site i and month j respectively. The total number of observations ($i \times j$) was 179

(Table 1) and the number of parameters varied between the four model variants, ranging from three in model 1a to eight in model 2b. It is noted that the parameters C_{RMI} and K_{RMI} that define the position of the baseline for the computation of the RMI are calibrated during this process (in model variants 2a and 2b). The Generalised Reduced Gradient method (Lasdon and Waren, 1979) was used, which assumes that the objective function is a smooth nonlinear function of the variables. When this is the case, it provides a fast way to find a minimum. In order to avoid the parameterisation reaching a local minimum only, the calibration procedure was repeated 1000 times. In each repetition the initial parameter values were randomly determined and the combination of parameters that yielded the lowest J , and satisfied the Kuhn-Tucker conditions of convergence was chosen. These conditions ensure that no small allowable change in the parameters can improve the objective function (Lasdon and Waren, 1979).

Model performance evaluation

We calculated the root mean square error (RMSE), the coefficient of determination (R^2) of the observed and modelled AET and the Nash-Sutcliffe coefficient of efficiency (E) (Nash and Sutcliffe, 1970) as:

$$E = 1 - \frac{\sum_i (AET_{O_i} - AET_{M_i})^2}{\sum_i (AET_{O_i} - \bar{AET}_O)^2} \quad (14)$$

The coefficient E is a measure of model performance and can range from $-\infty$ to 1. An efficiency of 1 corresponds to a perfect match of modeled and observed data. An efficiency of 0 indicates that the model predictions are as accurate as the mean of the observed data, and a negative efficiency occurs when the observed mean is a better predictor than the model. When the R^2 and E are equal the model predicts the observations with no bias and the unexplained variance ($1 - R^2 = 1 - E$) is caused by model error. When the R^2 is higher than E the difference between the two indices can be interpreted as a measure of model bias. For each model configuration we reported RMSE, R^2 and E for the seven sites taken simultaneously and also for each site taken separately.

We carried out a model cross validation by excluding each respective site from the calibration data and calculating the AET estimated for that site with the parameters obtained after calibrating the model against the remaining six sites (i.e. jack-knifing). This allowed us to assess the dependency of the model parameters on a specific calibration site.

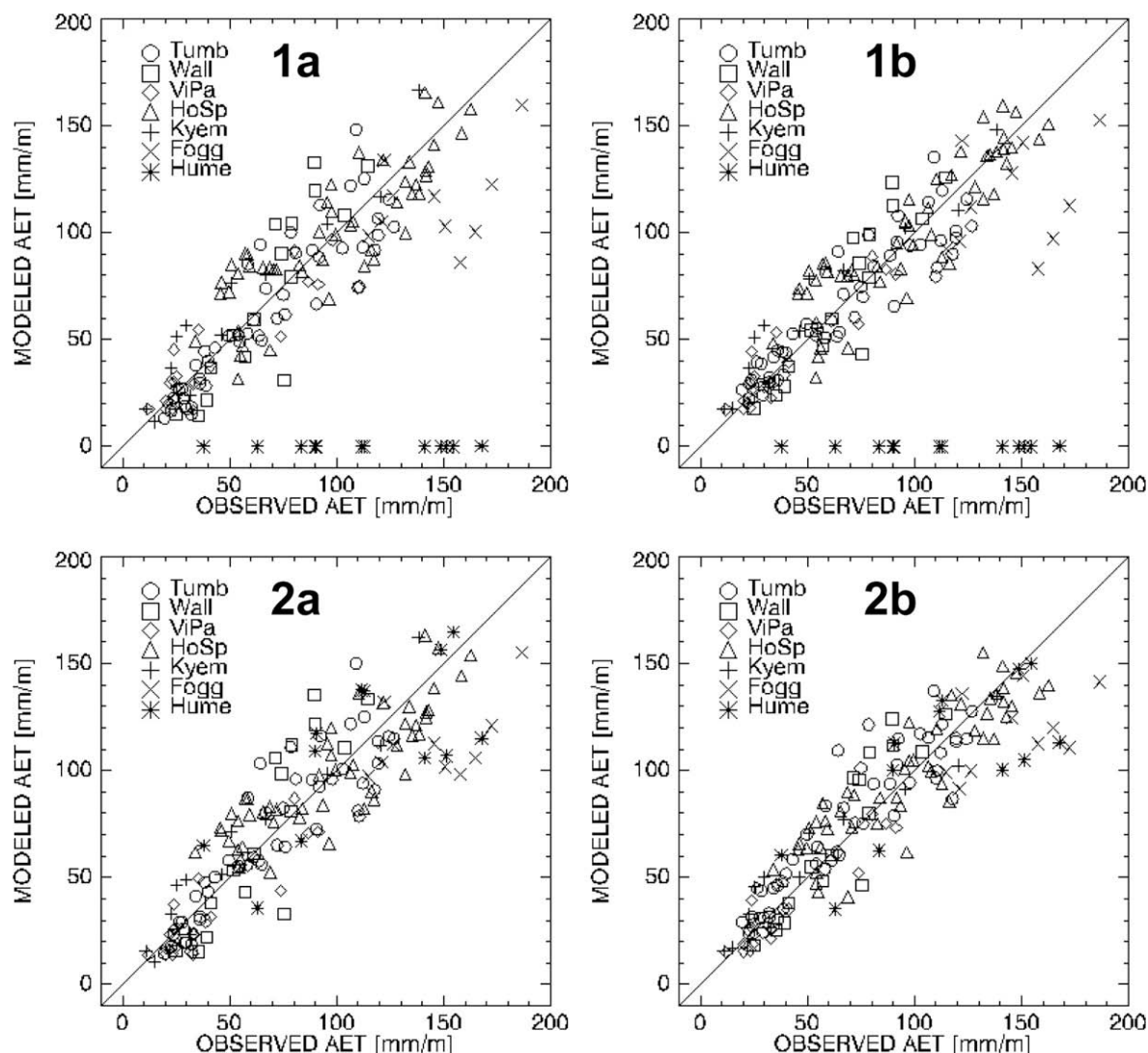


Fig. 3. Scatterplots showing predicted vs. observed AET in the seven field sites used for model calibration. Model variants 1a and 1b include a precipitation interception term and model variants 2a and 2b include a remote sensing index of surface moisture. The diagonal line in each graph indicates the 1:1 line.

We also tested the model performance by applying the calibrated model to an independent observational dataset. We used a streamflow data set for small catchments around Australia collated by Peel et al. (2000) and recently extended by Chiew et al. (in prep.) (Fig. 1). We compared average model estimated AET for a four year period (October 2001 to September 2005) to the difference between catchment average precipitation and end-of-catchment streamflow for the same period and also, the estimated net excess precipitation (precipitation minus model estimated ET) with the recorded average streamflow. The reason for selecting this period is that the spring season of those years had similar precipitation totals in south-east Australia, where the majority of the catchments are located, hopefully minimising the potential differences in soil and groundwater storage between the initial and final period. Full implications of this assumption are discussed further on. We selected those catchments with complete records for the selected period ($n = 227$, mean area = 484 km², range = 51 – 1979 km²). All catchments were unimpaired, i.e. were not significantly affected by regulation structures or streamflow extraction. We also compared the estimated net excess precipitation (precipitation minus model estimated ET) with the recorded average streamflow for the same period. The accuracy and/or bias in streamflow gauging may be assumed to be in the order of 10% over a longer period (i.e. around 10 years) (Peel et al., 2000). Where streamflow is a relatively small fraction of precipitation, errors in estimated period-average precipitation are a more likely source of uncertainty in our comparison.

Results

Assessment of alternative models

Model performance increased from model 1a to model 2b (Fig. 3 and Table 2). The simplest model formulation (1a), which used only the EVI and did not include a precipitation interception term performed well ($E > 0.7$) in the forest and grassland sites with the exception of Wallaby Creek where it had a high R^2 but low E indicating bias in the estimation. The model estimated AET very poorly at the wetland and open water sites, showing a negative E . When the precipitation interception term was added to the model formulation (model 1b) AET was estimated more accurately in the vegetated sites, particularly in Wallaby Creek. At this site, the EVI had a very weak correlation ($r = 0.01$) with the AET/PET ratio and consequently models 1a and 2a estimated AET with low efficiency. The fact that the R^2 between observed and modelled values was high in those model variants is reflecting the ability of the model to capture the seasonal pattern of AET. Because monthly precipitation has a strong correlation with the AET/PET ratio ($r = 0.78$), the inclu-

sion of the precipitation interception term in this site improved model efficiency. The performance of this model variant was however still very poor in the floodplain and open water sites. In Hume Dam model variants 1a and 1b estimated an AET of zero for all months (Fig. 3).

The inclusion of the residual moisture index in the estimation of the PET scaling factor (models 2a and 2b) resulted in an improvement of the estimated AET, particularly in the floodplain and open water sites and to a lesser extent in the grassland site. Model performance in those two sites, however, remained lower than in the forest and grassland sites and in Fogg Dam R^2 remained much higher than E indicating a strong bias in modelled AET. The most comprehensive model (2b) explained 82% of the variability in the observed AET (Table 2) with a mean square root error (RMSE) of 18 mm mo⁻¹ (22% of the mean AET) when all sites were considered simultaneously. This model variant effectively reproduced the seasonal patterns of AET at all sites (Fig. 4). No systematic over or underestimation occurred, with the exception of the Fogg Dam site where AET was underestimated during the year when compared with observed AET data.

Table 3 shows the values of the estimated parameters in each model variant. The parameters associated to the scaling of the EVI (a and α) were relatively stable between the four variants. The parameter $k_{C_{max}}$ which represents the maximum monthly crop factor k_C when the rescaled EVI or the RMI reach its maximum was 0.91 and 0.87 in the two model variants which did not include the precipitation interception term (1a and 2a). When the precipitation term was included (variants 1b and 2b) $k_{C_{max}}$ decreased to 0.76 and 0.68 and $k_{C_{max}}$ was 0.21 and 0.23 respectively. The parameters associated with the Residual Moisture Index were different between variants 2a and 2b. For example, the position of the baseline that defines the index changed its intercept and slope between model variants 2a and 2b. The scaling of the RMI into the k_C , determined by the parameters b and β also changed between the two variants, suggesting an interdependency of these parameters.

Model performance evaluation

Removing data from individual sites from the calibration dataset had different effects on the ability of the model in predicting AET in that particular site. For example when Virginia Park (open savanna) was not used for model calibration the resulting model could predict AET for that site with the same accuracy as when it was included (Table 2). The same occurred in Wallaby Creek and Kyemba. In contrast, the model predicted AET in the remaining sites much worse when those sites were removed from the calibration dataset. This was particularly evident in Howard Springs (open forest savanna), Fogg Dam (floodplain) and Hume Dam (open

Table 2

Performance of the AET model variants in the calibration sites. We report the root mean square error (RMSE), coefficient of determination (R^2) and Nash-Sutcliffe coefficient of efficiency (E). The last column (cross validation) shows the RMSE and R^2 for each site obtained by model 2b when that site was not used for model calibration.

SITE	Mean AET [mm mo ⁻¹]	n	Model 1a: no E_i , no RMI			Model 1b: E_i , no RMI			Model 2a: no E_i , RMI			Model 2b: both E_i and RMI			Cross-validation (model 2b)	
			RMSE [mm mo ⁻¹]	R^2	E	RMSE [mm mo ⁻¹]	R^2	E	RMSE [mm mo ⁻¹]	R^2	E	RMSE [mm mo ⁻¹]	R^2	E	RMSE [mm mo ⁻¹]	R^2
Tumb	68.3	49	15.7	0.81	0.78	13.5	0.84	0.83	15.5	0.81	0.78	15.0	0.84	0.80	18.3	0.83
Wall	67.9	16	22.5	0.78	0.16	16.8	0.84	0.53	23.9	0.78	0.05	17.7	0.84	0.48	20.4	0.83
ViPa	37.5	20	10.8	0.79	0.79	8.9	0.86	0.86	12.0	0.80	0.75	9.4	0.87	0.84	9.5	0.87
HoSp	97.3	49	19.2	0.72	0.72	16.4	0.80	0.79	18.4	0.75	0.74	16.2	0.80	0.80	31.4	0.54
Kyem	54.4	12	17.1	0.92	0.82	15.6	0.92	0.85	13.7	0.93	0.89	12.4	0.93	0.91	13.4	0.92
Fogg	146.1	10	40.3	0.12	-2.02	41.2	0.07	-2.15	38.7	0.21	-1.78	35.1	0.25	-1.29	43.6	0.10
Hume	112.6	12	119.2	0.18	-8.31	119.1	0.18	-8.31	29.2	0.50	0.44	28.5	0.54	0.47	62.1	0.52
All	79.9	168	37.1	0.42	0.25	36.1	0.43	0.29	20.1	0.78	0.78	18.	0.82	0.82		
All excluding Fogg & Hume	72.6	146	17.4	0.81	0.80	14.6	0.86	0.86	17.1	0.82	0.80	14.9	0.86	0.85		

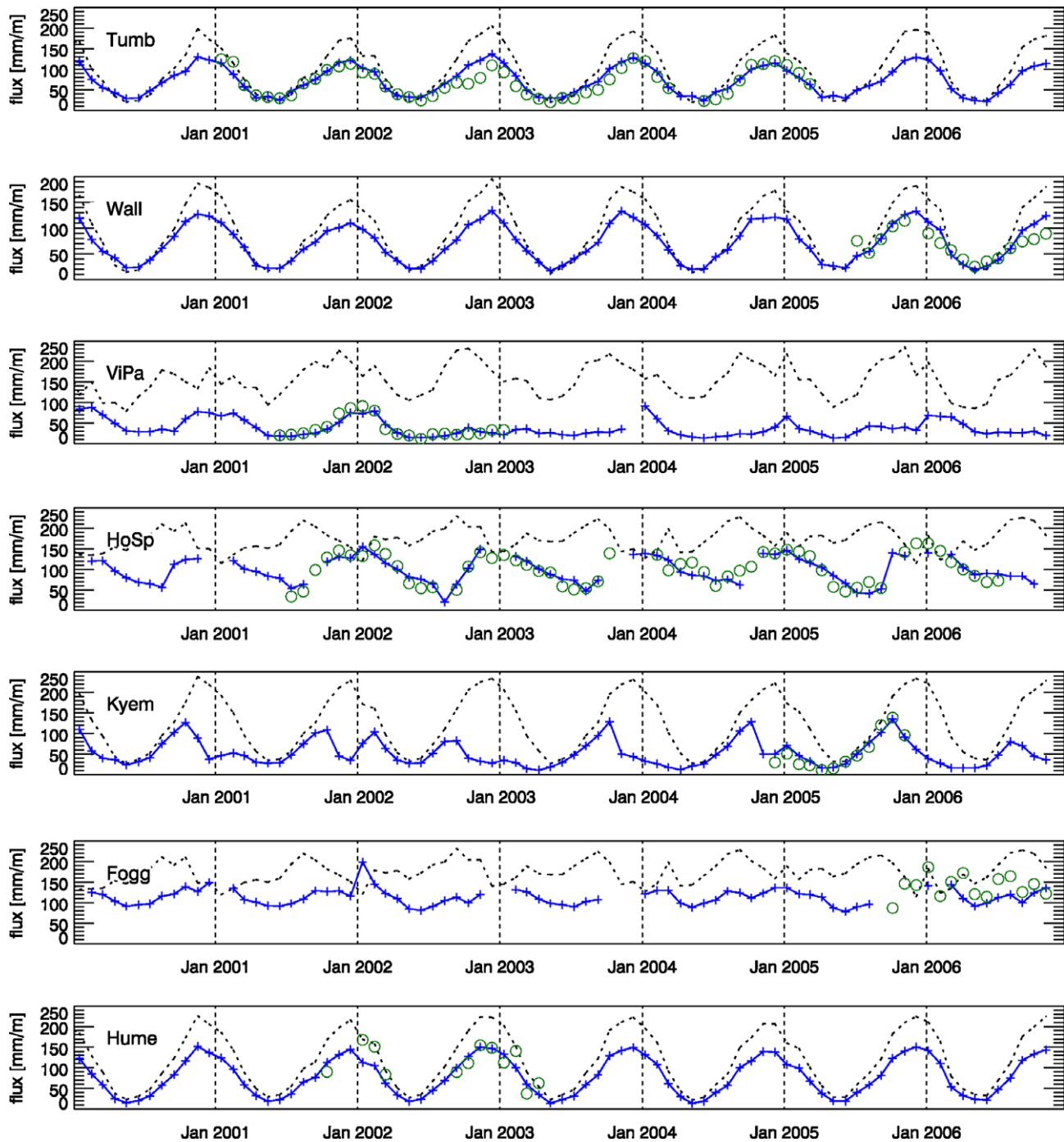


Fig. 4. Monthly Potential Evapotranspiration (dashed line), modeled AET (plus sign) and observed AET (circles) estimates in seven sites in Australia from 2000 to 2006. Missing data in the modeled AET was caused by missing remote sensing data likely caused by cloud contamination in the MODIS data, not removed by the compositing method. The AET model used here corresponded to model variant 2b.

water). These results reflect the importance of each particular site in the calibration of the model. However this could be simply indicating a leverage effect, dependent on the number and magnitude of observations.

When the calibrated models from the four model variants were applied to the evaluation dataset from 227 unimpaired catchments across Australia a similar pattern was observed: the models performed better when the precipitation interception term and/or the RMI were incorporated into the model formulae (Table 4). Model 2b explained 61% of the spatial variability of mean AET (between October 2001 and September 2005) (Fig. 5) with a RMSE of

137.4 mm mo^{-1} (19% of mean AET). Model efficiency was lower than the R^2 indicating that the model slightly overestimated AET. However, the origin and slope of the linear regression between predicted and observed values were not significantly different from 0 and 1 respectively ($p > 0.05$).

The estimated streamflow also improved from model variants 1a to 2b (Table 4) (note that modelled streamflow was assumed to equal zero when mean annual AET exceeded mean annual P). The RMSE of the predicted streamflow in all model variants was similar to the mean observed streamflow, indicating a high dispersion of the modelled values around the 1:1 line. The R^2 of the mod-

Table 3

Calibrated parameter values in the four model variants and range of values on which the parameters were allowed to vary during the parameterisation process.

Parameters	Model variant				Constraints	
	1a	1b	2a	2b	Min	Max
k_{MAX}	0.911	0.756	0.868	0.680	0	1
a	10.22	14.00	14.42	14.12	0	$+\infty$
α	2.38	2.458	2.701	2.482	0	$+\infty$
b			2.086	7.991	0	$+\infty$
β			0.953	0.890	0	$+\infty$
k_{EL_MAX}		0.207		0.229	0	1
K_{RMI}			1.778	0.775	0.5	2
C_{RMI}			−0.350	−0.076	−0.35	0.05

elled and predicted values was high (0.82) and similar to E , but was heavily influenced by seven catchments with high mean annual streamflow (located in Tasmania and Queensland).

Discussion

Assessment of alternative model structures

A large number of studies have shown that vegetation indices (VIs) can be satisfactorily used for estimating AET in agricultural crops (e.g. (Allen, 2000; Choudhury, 1994; Hunsaker et al., 2005)) and in natural vegetation (e.g. Nagler et al., 2007b; Nagler et al., 2005; Nagler et al., 2007a; Yang et al., 2006b). There are two main improvements on the VI approach presented in this paper. Firstly, incorporating a term that accounts for evaporation of intercepted precipitation improved the estimation of AET in the vegetated sites. For example the RMSE decreased from model variants 1a

to 1b between 1.4 and 5.7 mm mo^{−1} in the forest and savannas sites (Table 2). In the open water and floodplain sites the inclusion of the precipitation interception term did not change the model ability to estimate AET. Precipitation interception can account for 30–40% of total annual precipitation in temperate and tropical forests, depending on leaf area index, vegetation type and precipitation type and intensity (Bruijnzeel, 1997; Roberts, 1999). In the two forests sites included here observed AET was higher than PET in 5 out of 49 months (Tumbarumba) and in 5 out of 16 months (Wallaby Creek), suggesting a high proportion of water evaporated through precipitation interception. We showed that this process can be incorporated into remote sensing estimations of AET through the use of a simple, linear term depending on the EVI. Including a precipitation interception term also improved AET estimated at the catchment scale using an independent dataset (Table 4), providing some further support for the importance of this process also at larger scales.

We further conclude that a moisture index derived from reflective remote sensing data (RMI) can be used for estimating AET in open water areas (Hume Dam) and also improves AET estimation in those land cover types where standing surface water can be an important contribution to total evapotranspiration (Fogg Dam) (Table 2). The inclusion of the RMI did not improve the ability of the model to estimate AET in vegetated environments. The RMI functioned in the model as a means for discriminating pure open water pixels. Complementary analyses (not shown) suggest that the RMI is able to detect open water in mixed pixels, but this needs further research. Despite the improvement from including the RMI, these two sites still showed the highest errors and bias in AET prediction. A close inspection of the possible explanations of this suggested different causes. In Hume Dam (open water) the observed

Table 4

Performance of the four model variants in the catchments used for evaluation. The first row shows the performance of the model when the predicted AET was compared to the catchment water balance (mean difference between observed precipitation and streamflow). The second row shows the model performance when it used for estimating catchment streamflow (mean precipitation minus modelled AET). In this case modelled streamflow was assumed zero when mean AET was higher than mean precipitation.

Flux	Mean flux [mm/y]	n	Model 1a			Model 1b			Model 2a			Model 2b		
			RMSE [mm/y]	r^2	E	RMSE [mm/y]	r^2	E	RMSE [mm/y]	r^2	E	RMSE [mm/y]	r^2	E
AET	720.38	227	165.51	0.46	0.39	157.49	0.52	0.40	149.61	0.52	0.45	137.44	0.61	0.49
Streamflow	139.70	227	142.72	0.80	0.80	143.04	0.81	0.80	132.69	0.83	0.82	129.67	0.85	0.81

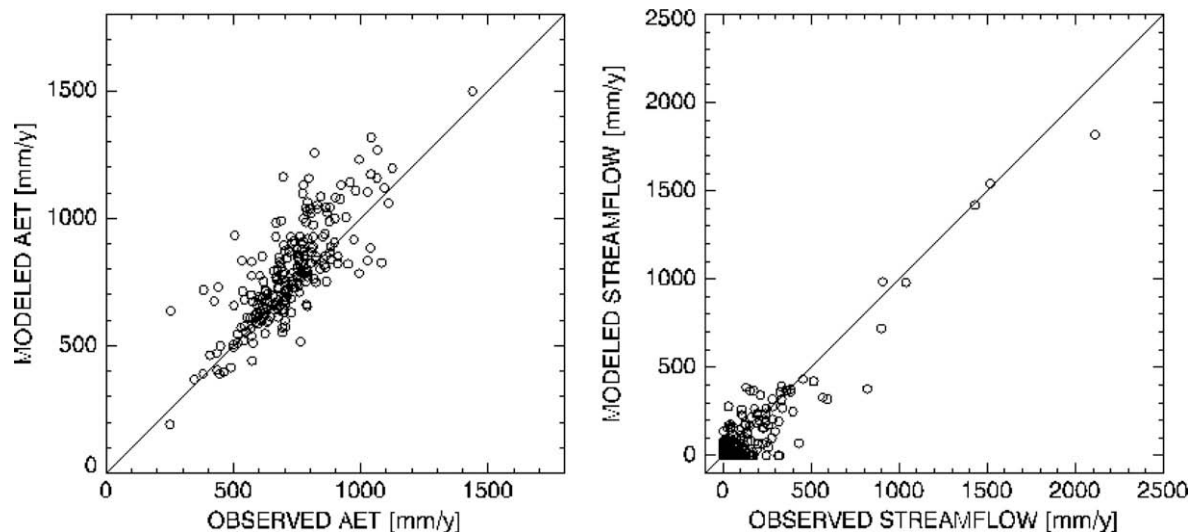


Fig. 5. Scatterplots showing modelled vs. observed mean (2001–2005) AET (left) and mean streamflow (right) in 227 unimpaired catchments in Australia. The results correspond to model variant 2b. Modelled streamflow was assumed to be zero when mean annual AET was higher than mean annual precipitation.

AET/PET ratio had a very low correlation with both the EVI and the GVMI (and thus the RMI). The inclusion of the RMI in the calculation of k_c (model variants 2a and 2b) allowed us to detect this site as an open water surface (Fig. 2) but did not capture the temporal dynamics of AET. Consequently, the model could estimate AET with less bias, but still failed to provide a good estimate of the seasonal patterns of AET. At the Fogg Dam site observed AET had an erratic behaviour and was not accurately captured by the EVI and GVMI (and the derived RMI) indices. This site features a dynamic fluctuation in surface water from the wet to dry seasons, with the dam filling once the cracking clay soils reaching saturation with the onset of the monsoon in December and January. Water depth ranges from 0.5 to 1 m depending on the magnitude of the monsoon. After March–April water levels begin to rapidly drop and by the late dry season (August–October) all surface water has evaporated. As such the site moves from an open water system with vegetation (grasses and sedges) to a drier, vegetation only system by the late dry season, with no free-standing water. The GVMI did not capture this seasonality possibly because the dense vegetation obscured the standing water and the site followed an EVI temporal dynamic more similar to the open forest savanna site (Fig. 2). Modelled AET is more consistent in the late dry seasons than the wet season (Fig. 4), where departures between modelled and observed data are evident.

Model performance evaluation

The overall accuracy achieved by the model proposed here is similar or better than those obtained by other remote sensing estimates of AET at weekly or monthly temporal resolutions. Using a semi-empirical model Cleugh et al. (2007) estimated 8-day AET with a RMSE of 28.3 mm mo^{-1} in the Tumbarumba and Virginia Park sites (two of the sites used here). Mu et al. (2007) improved Cleugh et al.'s model for a global MODIS product and achieved an identical RMSE (28.3 mm mo^{-1}) for 19 flux towers in North America. Using the same flux tower network as Mu et al. but an empirical model Yang et al. (2006b) achieved an 8-days RMSE of 20.7 and 17.3 mm mo^{-1} in forest and non-forest sites respectively. It is worth noting that the studies cited above did not include open water sites in their calibration or evaluation.

The temporal scale of observations and predictions influences the magnitude of prediction error. We compared the distribution of the differences between model predictions and observations at

the original temporal scale (one month) and aggregated at three, six and twelve months (Fig. 6). Relative differences in AET estimates decreased as the averaging period increased from one to six months and remained similar when considering a one year average. At the temporal scales analysed here (monthly to annual) the vegetation greenness detected by the EVI (associated to LAI) is largely responding to soil moisture availability, similarly to AET. This explains the good predictive ability of the simplest model (1a) in the vegetated sites. At the temporal scale of hours or days, in contrast, AET is more responsive to the micrometeorological conditions that determine plant water content and stomatal conductivity, which are not efficiently captured by vegetation indices of greenness (EVI or NDVI). Using remote sensing measures of land surface temperature has been the most common way to overcome this scaling issue (Van Niel and McVicar, 2004; Kalma et al., 2008). We speculate that the incorporation of an index like the GVMI (and the derived RMI) that captures vegetation and/or surface moisture content through the use of the shortwave infrared reflectance, could improve the estimation of AET at daily scales. Future studies should explore this alternative using, for example, daily MODIS-Terra and Aqua data simultaneously.

Few studies have used streamflow data as an evaluation (or calibration) source of a remote sensing-based evaporation method. Some authors have used catchment evaporation (the long-term difference of precipitation and runoff) as a means of comparing or evaluating AET estimated with sap-flow or eddy-covariance methods (Ford et al., 2007; Kosugi and Katsuyama, 2007; Wilson et al., 2001). In the remote sensing area Zhang et al. (2008) used long-term mean AET from 120 unimpaired catchments in the Murray-Darling basin of Australia (a subset of the catchments used in this paper) to calibrate the semi-empirical model of Leuning et al. (2008) driven by MODIS and meteorological data. Zhang et al. later used the model for estimating runoff and assumed a zero runoff when mean AET exceeded P . In order to compare our results to those of Zhang et al. we rerun the analyses using a subset of the catchment dataset using only the 77 catchments included in the Murray-Darling basin (the number of catchments was different in the study by Zhang et al. because we used an older version of the database). Mean annual AET was estimated with a RMSE of 78.6 mm y^{-1} ($\sim 12\%$ of the mean AET) by Zhang et al. and no bias. We obtained an almost identical value (79.3 mm y^{-1}) and also no significant bias. Regarding runoff, Zhang et al. obtained a RMSE

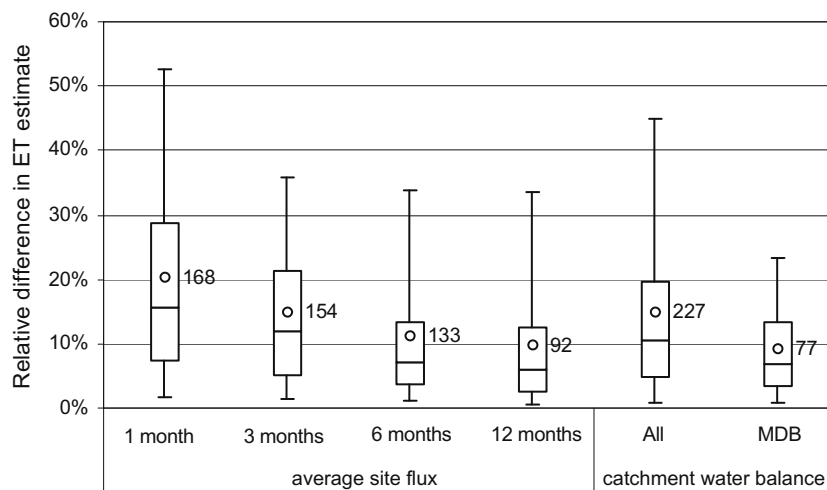


Fig. 6. The distribution of absolute values of the difference $|x_{\text{mod}}/x_{\text{obs}} - 1|$ between model estimates of ET and flux tower observations at seven sites (used for model calibration) over different averaging periods, and estimates from on a four-year water balance for a data set of catchments across Australia and in the Murray-Darling Basin (Murray-Darling Basin) (not used in calibration). Shown are quartiles (box), 5% outer percentiles (whiskers), average difference (circles) and the number of values.

of 71.0 mm y^{-1} , higher than the RMSE obtained by the model presented here (56.0 mm y^{-1}). Zhang et al. also demonstrated that remote sensing did better at estimating runoff than other methods

including hydrological catchment models. We conclude that the model presented here performs similarly compared with other studies which took a more process-based approach.

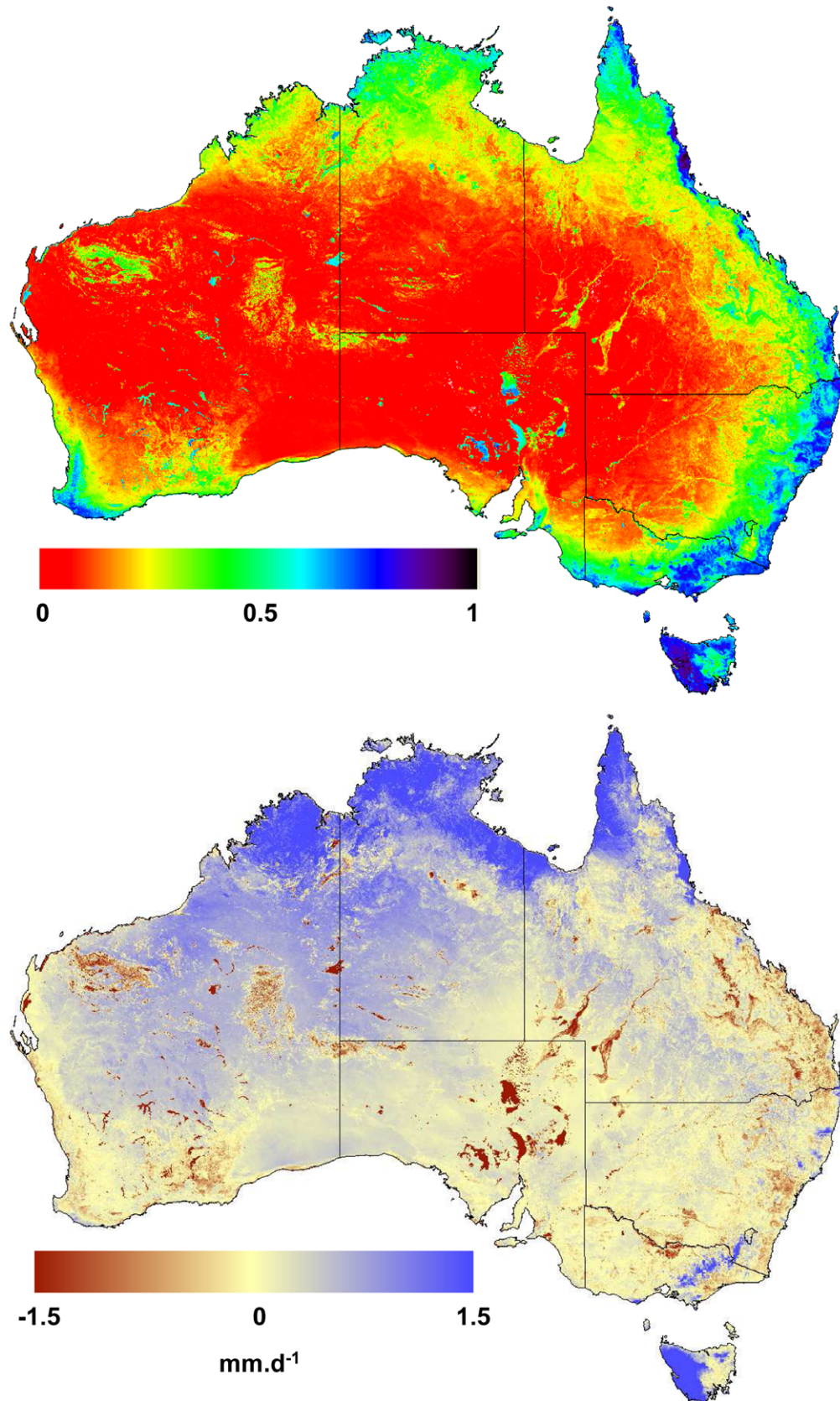


Fig. 7. Ratio of mean AET to mean PET (top) and difference between mean precipitation and mean AET (bottom) for the period 2000–2006.

The accuracy of the AET estimates derived depends on the uncertainty and bias from the model itself as well as those arising from the observations used as model inputs. In the model presented here we have identified or estimated uncertainties in the observations in the order of 10–20% (AET measurements, climate surfaces) which could lead to errors of the same magnitude as the model estimates. In addition, when comparing model outputs to data derived from streamflow measurements we assumed that changes in soil moisture between the beginning and end of the period considered were negligible. However, differences in soil moisture play a role, especially in highly seasonal sites, such as the savanna sites. A soil may have a plant available water storage capacity (between field capacity and wilting point) in the order of 20–50%, i.e. 200–500 mm per metre of soil, depending on texture. Similarly, there may be differences in groundwater storage, although baseflow analyses do not suggest these to be significant over the period considered in this study (Van Dijk, *pers. comm.*).

When the model 2b was applied to the entire Australian continent the general spatial patterns of AET were consistent with those shown by other global, continental and regional studies. For example, a qualitative comparison of Fig. 11 in Cleugh et al. (2007) and Fig. 7a in this paper show a similar spatial distribution of the ratio of AET/PET in Australia. The maps presented by Zhang et al. (submitted for publication) also show similar general spatial patterns. The dry interior of the continent had an AET/PET ratio close to zero and it increased in the coastal areas of the east, southwest and in Tasmania. The AET/PET ratio was high (close to 1) in the tropical rainforests of NE Queensland and in the western forests of Tasmania. Wetlands, ephemeral and permanent lakes were also evident in the map, showing a higher AET/PET ratio than the arid lands surrounding them (Fig. 7a). Mean annual water balance (the difference between mean P and AET) was positive in most of the north of the continent, in western Tasmania and in the mountain ranges of SE New South Wales and Victoria (Fig. 7b). It was highly negative in all lakes, wetlands and irrigated areas which evaporate, in addition to water received as precipitation, water from surface runoff and diversions.

The AET models developed here have shown good agreement with in situ observations of AET and with runoff measured in a large number of catchments. However, both the observations used for calibration and the catchments used for model evaluation are located in areas with mean annual precipitation higher than 250 mm y^{-1} . As a consequence, most of the Australian landmass (dominated by dry to very dry environments) is underrepresented in the calibration and evaluation datasets. However, the maps shown in Fig. 7 indicate similar AET and P in the dry environments and suggest that the water balance is closed in those areas.

Conclusions

A simple empirical model driven by climatic data and two indices derived from reflective MODIS data was able to estimate monthly actual evapotranspiration in seven sites in Australia. The model has one set of parameters for all land cover types and does not need a land cover classification as input data and consequently is not subject to errors of misclassification. Two key characteristics of the model are the inclusion of a term that explicitly represents precipitation interception losses and a remote sensing index of surface moisture. The former allowed to estimate AET with better accuracy in vegetated environments, particularly in forests and savannas. The latter was able to capture the presence of open water surfaces and improved the estimation of AET in an open water site and in a floodplain.

The model was able to reproduce the long-term spatial patterns of AET in 227 catchments used as independent testing data. In

those catchments the inclusion of the precipitation interception term and the surface moisture index also improved the ability of the model to estimate AET suggesting that, although of an empirical nature in the model formulation, the two model components capture essential features of the evaporation process at the landscape scale.

Acknowledgements

We are grateful to Damian Barrett and Tim McVicar who provided valuable comments on the manuscript.

References

- Alexander, L.V. et al., 2007. Trends in Australia's climate means and extremes: a global context. *Australian Meteorological Magazine* 56 (1), 1–18.
- Allen, R.G., 2000. Using the FAO-56 dual crop coefficient method over an irrigated region as part of an evapotranspiration intercomparison study. *Journal of Hydrology* 229 (1–2), 27–41.
- Beringer, J. et al., 2003. Fire impacts on surface heat, moisture and carbon fluxes from a tropical savanna in northern Australia. *International Journal of Wildland Fire* 12 (3–4), 333–340.
- Beringer, J., Hutley, L.B., Tapper, N.J., Cernusak, L.A., 2007. Savanna fires and their impact on net ecosystem productivity in North Australia. *Global Change Biology* 13 (5), 990–1004.
- Brujinzeel, L.A., 1997. Hydrology of forest plantations in the humid tropics. In: Nambiar, E.K.S., Brown, A.H. (Eds.), *Better Management of Soils, Nutrients and Water in Tropical Forest Plantations*. ACIAR, Canberra, pp. 125–167.
- Ceccato, P., Flasse, S., Gregoire, J.-M., 2002a. Designing a spectral index to estimate vegetation water content from remote sensing data: part 2. Validation and applications. *Remote Sensing of Environment* 82 (2–3), 198–207.
- Ceccato, P., Gobron, N., Flasse, S., Pinty, B., Tarantola, S., 2002b. Designing a spectral index to estimate vegetation water content from remote sensing data: part 1: theoretical approach. *Remote Sensing of Environment* 82 (2–3), 188–197.
- Choudhury, B.J., 1994. Synergism of multispectral satellite-observations for estimating regional land-surface evaporation. *Remote Sensing of Environment* 49 (3), 264–274.
- Cleugh, H.A., Leuning, R., Mu, Q., Running, S.W., 2007. Regional evaporation estimates from flux tower and MODIS satellite data. *Remote Sensing of Environment* 106 (3), 285–304.
- Deguchi, A., Hattori, S., Park, H.T., 2006. The influence of seasonal changes in canopy structure on interception loss: application of the revised Gash model. *Journal of Hydrology* 318 (1–4), 80–102.
- Doorenbos, J., Pruitt, W.O., 1977. Guidelines for predicting crop water requirements. FAO irrigation and drainage paper ; 24. FAO, Rome, xii, 144pp.
- Doraiswamy, P.C., Thompson, D.R., 1982. A crop moisture stress index for large areas and its application in the prediction of spring wheat phenology. *Agricultural Meteorology* 27 (1–2), 1–15.
- Falge, E. et al., 2001. Gap filling strategies for long term energy flux data sets. *Agricultural and Forest Meteorology* 107 (1), 71–77.
- Ford, C.R., Hubbard, R.M., Kloeppel, B.D., Vose, J.M., 2007. A comparison of sap flux-based evapotranspiration estimates with catchment-scale water balance. *Agricultural and Forest Meteorology* 145 (3–4), 176–185.
- Glenn, E.P., Huete, A.R., Nagler, P.L., Hirschboeck, K.K., Brown, P., 2007. Integrating remote sensing and ground methods to estimate evapotranspiration. *Critical Reviews in Plant Sciences* 26 (3), 139–168.
- Hobbins, M.T., Ramirez, J.A., Brown, T.C., 2001. The complementary relationship in estimation of regional evapotranspiration: An enhanced advection-aridity model. *Water Resources Research* 37, 1389–1403.
- Huete, A. et al., 2002. Overview of the radiometric and biophysical performance of the MODIS vegetation indices. *Remote Sensing of Environment* 83 (1–2), 195–213.
- Hunsaker, D.J., Barnes, E.M., Clarke, T.R., Fitzgerald, G.J., Pinter, P.J., 2005. Cotton irrigation scheduling using remotely sensed and FAO-56 basal crop coefficients. *Transactions of the Asae* 48 (4), 1395–1407.
- Jeffrey, S.J., Carter, J.O., Moodie, K.B., Beswick, A.R., 2001. Using spatial interpolation to construct a comprehensive archive of Australian climate data. *Environmental Modelling and Software* 16 (4), 309–330.
- Kalma, J.D., McVicar, T.R., McCabe, M.F., 2008. Estimating land surface evaporation: a review of methods using remotely sensed surface temperature data. *Surveys in Geophysics* 29, 421–469.
- Kosugi, Y., Katsuyama, M., 2007. Evapotranspiration over a Japanese cypress forest. II. Comparison of the eddy covariance and water budget methods. *Journal of Hydrology* 334 (3–4), 305–311.
- Lasdon, L.S., Waren, A.D., 1979. Generalized reduced gradient software for linearly and nonlinearly constrained problems. In: Greenberg, H. (Ed.), *Design and Implementation of Optimization Software*. Sijthoff and Noordhoff.
- Leuning, R., Cleugh, H.A., Zegelin, S.J., Hughes, D., 2005. Carbon and water fluxes over a temperate Eucalyptus forest and a tropical wet/dry savanna in Australia: measurements and comparison with MODIS remote sensing estimates. *Agricultural and Forest Meteorology* 129 (3–4), 151–173.

- Leuning, R., Zhang, Y.Q., Rajaud, A., Cleugh, H.A., Tu, K., 2008. A simple surface conductance model to estimate regional evaporation using MODIS leaf area index and the Penman-Monteith equation. *Water Resources Research* 44, W10419, doi:10.1029/2007WR006562.
- Liu, Y., de Jeu, R.A.M., van Dijk, A., Owe, M., 2007. TRMM-TMI satellite observed soil moisture and vegetation density (1998–2005) show strong connection with El Niño in eastern Australia. *Geophysical Research Letters* 34 (15).
- Martin, D., Beringer, J., Hutley, L.B., McHugh, I., 2007. Carbon cycling in a mountain ash forest: analysis of below ground respiration. *Agricultural and Forest Meteorology* 147 (1–2), 58–70.
- McVicar, T.R., Van Niel, T.G., Li, L.T., Roderick, M.L., Rayner, D.P., Ricciardulli, L., Donohue, R.J., 2008. Wind speed climatology and trends for Australia, 1975–2006: capturing the stilling phenomenon and comparison with near-surface reanalysis output. *Geophysical Research Letters* 35, L20403. doi:10.1029/2008GL035627.
- Morton, F.I., 1983. Operational estimates of areal evapotranspiration and their significance to the science and practice of hydrology. *Journal of Hydrology* 66, 1–76.
- Mu, Q., Heinsch, F.A., Zhao, M., Running, S.W., 2007. Development of a global evapotranspiration algorithm based on MODIS and global meteorology data. *Remote Sensing of Environment* 111 (4), 519–536.
- Murakami, S., 2006. A proposal for a new forest canopy interception mechanism: splash droplet evaporation. *Journal of Hydrology* 319 (1–4), 72–82.
- Myneni, R.B. et al., 2007. Large seasonal swings in leaf area of Amazon rainforests. *Proceedings of the National Academy of Sciences of the United States of America* 104 (12), 4820–4823.
- Nagler, P.L. et al., 2005. Predicting riparian evapotranspiration from MODIS vegetation indices and meteorological data. *Remote Sensing of Environment* 94 (1), 17–30.
- Nagler, P. et al., 2007a. Evapotranspiration in a cottonwood (*Populus fremontii*) restoration plantation estimated by sap flow and remote sensing methods. *Agricultural and Forest Meteorology* 144 (1–2), 95–110.
- Nagler, P.L. et al., 2007b. Relationship between evapotranspiration and precipitation pulses in a semiarid rangeland estimated by moisture flux towers and MODIS vegetation indices. *Journal of Arid Environments* 70 (3), 443–462.
- Nash, J.E., Sutcliffe, J.V., 1970. River flow forecasting through conceptual models part I – a discussion of principles. *Journal of Hydrology* 10 (3), 282–290.
- Nemani, R.R. et al., 2003. Climate-driven increases in global terrestrial net primary production from 1982 to 1999. *Science* 300 (5625), 1560–1563.
- Paget, M.J., King, E.A., 2008. MODIS Land data sets for the Australian region. CSIRO Marine and Atmospheric Research Internal Report No. 004. 96pp.
- Peel, M.C., Chiew, F.H.S., Western, A.W., McMahon, T.A., 2000. Extension of Unimpaired Monthly Streamflow Data and Regionalisation of Parameter Values to Estimate Streamflow in Ungauged Catchments. Report prepared for the Australian National Land and Water Resources Audit., Centre for Environmental Applied Hydrology. The University of Melbourne.
- Priestley, C.H.B., 1966. The limitation of temperature by evaporation in hot climates. *Agricultural Meteorology* 3 (3/4), 241–246.
- Priestley, C.H.B., Taylor, R.J., 1972. On the assessment of surface heat flux and evaporation using large-scale parameters. *Monthly Weather Review* 100, 81–92.
- Raupach, M.R., 1995. Vegetation–atmosphere interaction and surface conductance at leaf, canopy and regional scales. *Agricultural and Forest Meteorology* 73 (3–4), 151–179.
- Raupach, M. et al., 2001. Balances of Water, Carbon, Nitrogen and Phosphorus in Australian Landscapes: (2) Model Formulation and Testing, Canberra, Australia.
- Roberts, J., 1999. Plants and water in Forests and Woodlands. In: Baird, A.J., Wilby, R.L. (Eds.), *Eco-Hydrology: Plants and Water in Terrestrial and Aquatic Environments*. Routledge, London, p. 402.
- Schaaf, C.B. et al., 2002. First operational BRDF, albedo nadir reflectance products from MODIS. *Remote Sensing of Environment* 83 (1–2), 135–148.
- Schellekens, J., 2000. The interception and runoff generating processes in the Bisley catchment, Luquillo Experimental Forest, Puerto Rico. *Physics and Chemistry of the Earth Part B-Hydrology Oceans and Atmosphere* 25 (7–8), 659–664.
- Sherman, B., 2005. Hume Reservoir thermal monitoring and modelling – final. Report for State Water as agent for the Murrumbidgee Basin Commission. CSIRO Land and Water Client Report. CSIRO Land and Water, Canberra.
- Shuttleworth, W.J., Calder, I.R., 1979. Has the Priestley–Taylor equation any relevance to forest evaporation. *Journal of Applied Meteorology* 18 (5), 639–646.
- van Dijk, A., Bruijnzeel, L.A., 2001a. Modelling rainfall interception by vegetation of variable density using an adapted analytical model. Part 1. Model description. *Journal of Hydrology* 247 (3–4), 230–238.
- van Dijk, A., Bruijnzeel, L.A., 2001b. Modelling rainfall interception by vegetation of variable density using an adapted analytical model. Part 2. Model validation for a tropical upland mixed cropping system. *Journal of Hydrology* 247 (3–4), 239–262.
- Van Dijk, A., Dolman, A.J., 2004. Estimates of CO₂ uptake and release among European forests based on eddy covariance data. *Global Change Biology* 10 (9), 1445–1459.
- van Dijk, A.I.J.M., Keenan, R.J., 2007. Planted forests and water in perspective. *Forest Ecology and Management* 251 (1–2), 1–9.
- Van Dijk, A.I.J.M., Mestersdorf, G., 2007. Comparison of MODIS-based scaling of potential evapotranspiration with on-ground observations. *EGU 2007, Geophysical Research Abstracts* 9, 11692.
- Van Niel, T.G., McVicar, T.R., 2004. Current and potential uses of optical remote sensing in rice-based irrigation systems: a review. *Australian Journal of Agricultural Research* 55 (2), 155–185.
- Wallace, J., McJannet, D., 2008. Modelling interception in coastal and montane rainforests in northern Queensland, Australia. *Journal of Hydrology* 348 (3–4), 480–495.
- Wilson, K.B., Hanson, P.J., Mulholland, P.J., Baldocchi, D.D., Wullschlegel, S.D., 2001. A comparison of methods for determining forest evapotranspiration and its components: sap-flow, soil water budget, eddy covariance and catchment water balance. *Agricultural and Forest Meteorology* 106 (2), 153–168.
- Wilson, K. et al., 2002. Energy balance closure at FLUXNET sites. *Agricultural and Forest Meteorology* 113 (1–4), 223–243.
- Wood, S.A., Beringer, J., Hutley, L.B., McGuire, A.D., Van Dijk, A., Kilinc, M., 2008. Impacts of fire on forest age and runoff in mountain ash forests. *Functional Plant Biology* 35, 483–492.
- Xiao, X. et al., 2002. Observation of flooding and rice transplanting of paddy rice fields at the site to landscape scales in China using VEGETATION sensor data. *International Journal of Remote Sensing* 23 (15), 3009–3022.
- Yang, F.H. et al., 2006. Prediction of continental-scale evapotranspiration by combining MODIS and AmeriFlux data through support vector machine. *IEEE Transactions on Geoscience and Remote Sensing* 44 (11), 3452–3461.
- Zhang, Y.Q., Chiew, F.H.S., Zhang, L., Leuning, R., Cleugh, H.A., 2008. Estimating catchment evaporation and runoff using MODIS leaf area index and the Penman-Monteith equation. *Water Resources Research*, in press, doi:10.1029/2007WR006563.